Research on Engineering Structures & Materials
www.jresm.org
Research Group

Research Article

Enhancing structural integrity of plastic concrete diaphragm walls in dams on thick alluvium: A numerical study of geometry and construction sequencing

Idrissa Ouedraogo[*,1,a], Anas Bahi [1,b], Latifa Ouadif [1,c]

L3GIE Laboratory, Mohammed V University, Mohammadia Engineering School, 10090 Agdal Rabat, Morocco

Article Info

Article History:

Received 30 Apr 2025

Accepted 28 July 2025

Keywords:

Concrete Face Rockfill Dam;
Alluvium;
Plastic concrete;
Diaphragm wall;
Geometric optimization;
Stress concentration;
Junction;
Junction angle;
Distortion

Abstract

Diaphragm walls are particularly useful in Dams laying on thick alluvial valleys, making it possible to connect the watertight components of the structure to the deep bedrock. This article analyses the case of a Concrete Face Rockfill Dam, resting on approximately 35 m of alluvium, where a soft concrete diaphragm wall was built to overcome tightness issues caused by the alluvium layer. The paper recalls the behavior of a plastic concrete diaphragm wall to analyze its dimensioning parameters, in order to propose a geometrically based design improvement. The study is based on numerical simulation, using Plaxis software. It emerges from the study that the area connecting the wall to the watertight organs of the dam constitutes its most critical part, where distortions reach 2%. The article thus proposes a softening of this junction. This design makes it possible to significantly reduce the concentration of deformations in that area. Applying this solution brings down the distortion to only 0,1%. Plus, the study shows that better results can be reached by having a strategic planning of the dike construction.

1. Introduction

Dams are artificial barriers constructed in watercourses to create reservoirs for diverse purposes, including agriculture, hydroelectric power, domestic water supply, flood control, and recreational activities [1, 15]. However, geological investigations sometimes reveal challenges related to the watertightness of dam foundations. The Rhiss Dam in northeastern Morocco serves as the subject of this study. Geological assessments utilizing methods such as drilling and geophysical surveys have identified that the valley is filled with alluvial deposits overlying bedrock, reaching depths of up to thirty-five meters [5]. These alluvial soils, though recognized as productive and valuable for various uses, pose significant geotechnical challenges for dam foundations due to their permeability and high deformability [6, 7]. These characteristics not only compromise structural stability but also raise concerns related to soil liquefaction, especially in saturated conditions [1]. To address such risks, investigated vibro-compaction as a ground improvement technique for a similar sandy foundation in a Moroccan port area, suggesting important design parameters [14]. Liquefaction, a transient loss of soil strength in saturated conditions, has been characterized as a severe geohazard by Berkat et al. [16].

In response to seepage issues through alluvial foundations, Ouedraogo studied the use of a plastic diaphragm wall as a watertight barrier [1]. According to Hruban [17], such a diaphragm wall is "a wall constructed in a trench excavated mechanically from the surface", and it has been applied in various civil engineering contexts particularly for the formation of cofferdams to prevent seepage.

[*]Corresponding author: idr.oued07@gmail.com
[a]orcid.org/ 0009-0001-9410-7102; [b]orcid.org/ 0000-0002-1450-7254; [c]orcid.org/0000-0002-4613-1124;
DOI: http://dx.doi.org/10.17515/resm2025-858st0430rs

The structural behavior and performance of diaphragm walls have been the subject of several recent investigations. For instance, Jingwu Zhang et al., [2] analyzed lateral earth pressures on circular diaphragm walls and validated their analytical model with the Beam on Nonlinear Elastic Foundation (BNEF) method proposed by Wei He et al [3] Meanwhile, Yong Shao et al., [4] addressed leakage detection using Fiber Bragg Grating (FBG) sensing technologies. Despite these contributions, a specific phenomenon observed by Ouedraogo et al. [1] remains insufficiently explored: the accumulation of deformations at the junction between the concrete head block and the diaphragm wall body (Fig. 1). This localized distortion could critically affect the structural integrity of the diaphragm wall, yet few studies have quantitatively assessed or modeled its development.

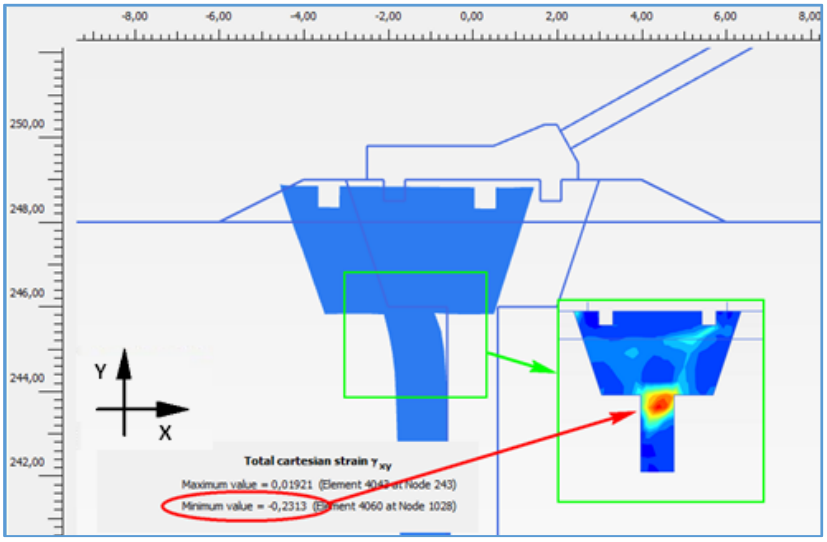

Fig. 1. Distortion accumulating in the junction of the concrete head block and the body of the diaphragm wall (adapted from [1])

The present study aims to investigate the deformation patterns observed at the junction between the concrete head block and the diaphragm wall, particularly in the context of thick alluvial layers such as those at the Rhiss Dam site. Using numerical modeling, the research simulates displacement and distortion fields within the diaphragm wall system, offering a detailed assessment of the structural behavior under geotechnical loading. The results confirm the presence of significant distortion concentrations at the junction points, reaching up to 2%, which pose a threat to the long-term performance of the wall. In response, two design optimizations were proposed. Most notably, smoothing the junction angle between the head block and the diaphragm wall body—a simple and cost-effective measure proved highly effective. This modification reduced the distortion at the upper junction point from 2% to just 0.1%, and also mitigated a secondary distortion peak at mid-height of the wall from 2.1% to 0.45%. These findings not only validate the initial observations by Ouedraogo et al. [1] but also offer practical engineering strategies to improve diaphragm wall integrity in similar geotechnical settings.

2. Materials and Methods

The subject of our investigation is the identical case as Ouedraogo et al. [1]. We adhered to a strict protocol that included bibliography research and comparisons of numerical analysis in order to achieve our original objective, which is to reduce the concentration of distortions at the junction points of the diaphragm wall (as it appears on Fig. 1). The analyses are made using Plaxis software.

2.1. Design of the Dam and the Diaphragm Wall

The paper investigates on a CFRD Dam (Concrete Faced Rockfill Dam). It was designed in accordance with the suggestions made by the CFBR (Comité Français des Barrages et Retenues) and the International Commission On Large Dams (ICOLD). The Dam's other components have

designed accordingly to [9, 10,12,13], which are indications provided by CIGB-ICOLD and CFBR for the design of CFRD dam components.

The dam is 85m high (with 8m crest) and laying on 35m of alluvium layer. The upstream facing is 1,8H/1V and the downstream facing is 2,35H/1V. Under the alluvium is the bedrock, composed of shale clay. Souileh et al., [18] found a permeability of $2.5x10^{-6}$ m/s for Khouribga shale clay, showing the tightness of that rock. The bedrock is indeed supposed to be watertight and incompressible. To connect the concrete face to the bedrock, a complex of plinth-concrete head block-diaphragm wall is constructed. The plinth and the concrete face are made with reinforced concrete while the diaphragm wall and its head block are in plastic concrete. This concept was explained by Ouedraogo et al, in his study [1].

The Dam was constructed using alluvium in the reservoir and shale clay from the bedrock. This has been made as ecofriendly procedure in order to utilize local construction materials. For instance, shale clay is encouraged to be used nowadays in Morocco, and prove high performance when used in concrete formulation. Indeed, Souileh et al., [19] found that clay shale-based concrete achieved a compressive strength of 12 MPa after seven days and 16 MPa after 28 days, meeting B25 concrete standards.

The diaphragm wall was constructed using a stair-step foundation that ensures a minimum anchoring of 1 m in the bedrock, and alternating main and secondary studs that are around 7 m wide each. It crosses the whole alluvium layer (35m) with 1m encoring in the shale bedrock. A layer of clayey silts, followed by a layer of coarse alluvium and finally a layer of alluvium, covers the fine (filtering) material that protects the concrete head block upstream. A cross-section of the diaphragm wall is shown in Figure 2.

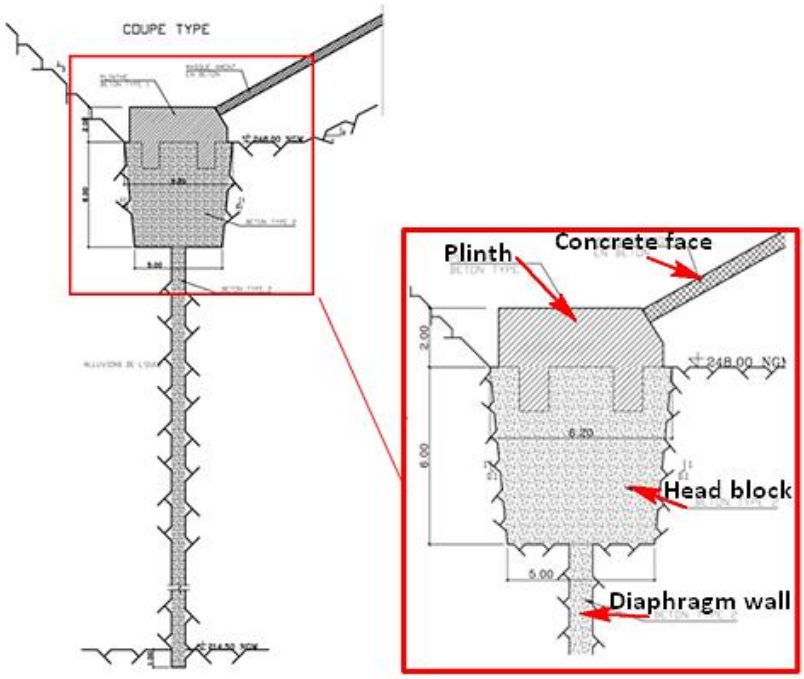

Fig. 2. Typical section of the diaphragm wall (adapted from [1])

In the current study, this conception has been maintained in order to be compared with an all-new design. This new design (solution 1. See §3.2) is indeed an enhanced one that makes it possible to mitigate distortions concentration at the junction point.

2.2. Numerical Analysis

We have employed finite elements-based numerical analysis to evaluate the diaphragm wall's capacity to withstand the constraints that it faces, where the loads listed below have been considered: water pressure and ground push and stop.

According Ouedraogo et al., [1], the water in the reservoir exerts a hydrostatic pressure equal to:

$$Pw = W.H \quad (1)$$

Where Pw is the hydrostatic pressure, W is the volume mass of water (1t/m3), and H is hydraulic load. The anchoring of the watertight break (diaphragm wall) in the bedrock and the permeability of the various horizons determine the hydraulic load (H) downstream of the diaphragm wall. The model computes it automatically. Due to nearly complete head loss in the bedrock, it is nearly constant between the diaphragm wall's downstream and the dam's downstream toe, and it is equivalent to the water level upstream of the dam [1]. Based on materials deformation and their limit resistance, the stresses that the ground applies to the diaphragm wall are automatically determined. As a result, the following factors determine the thrust and stop forces [1:

- Moduli of ground deformation.
- The soil's cohesiveness and friction angle.
- The wall's inertia.

The materials used in the model are adapted from [1] and their properties are shown on Tab 1, while Figure 3 shows the model, as simulated on Plaxis software.

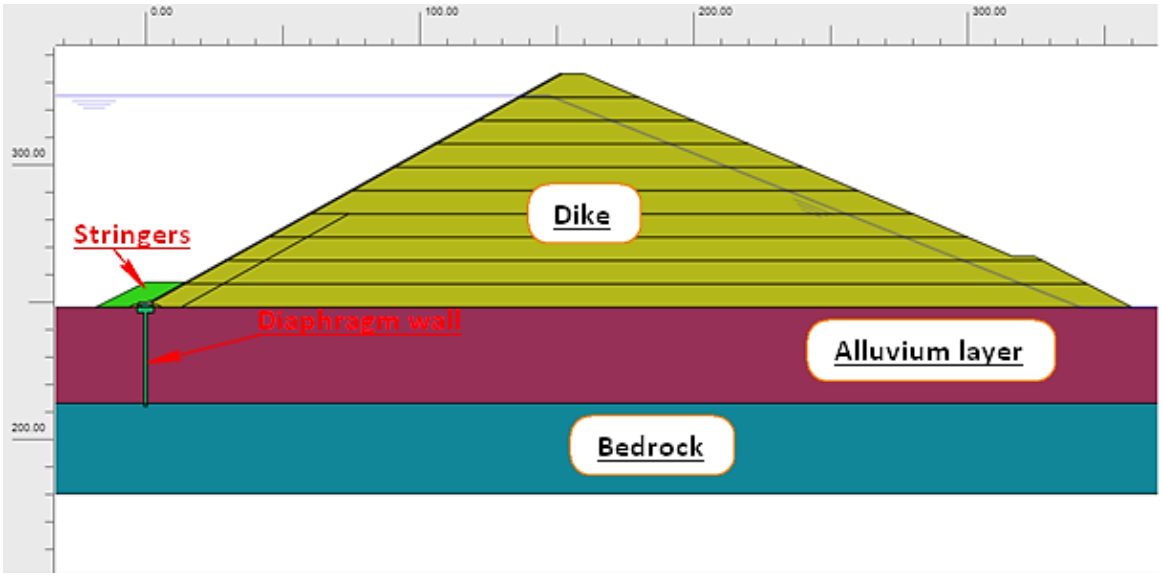

Fig. 3. Cross section of the model

Table 1. Materials used in the model and their parameters.

Materials	γ_{sec} (kN/m³)	n (%)	γ_{sat} (kN/m³)	K (m/s)	E (kN/m²)	C (kN/m²)	φ (°)	ν
Alluvium	21.0	10.0%	22.0	4.0E-05	2.0E+04	0.25*	39.00	0.25
Dike	23.2	10.0%	24.0	1.0E-04	1.0E+05	0.25*	39.00	0.3
Stringers	17.1	1.0%	17.20	1.0E-08	2.6E+04	50	26	0.19
Bedrock	21.0	1.0%	21.1	1.0E-09	3.0E+05	70	37.00	0.3
Diaphragm wall	23.2	1.0%	23.3	1.0E-08	4.0E+05	145	32	0.3
Plinth	24.5	0.1%	24.51	1.0E-11	2.2E+07	-	-	0.20
Concrete face	24.5	0.1%	24.51	1.0E-11	2.2E+07	-	-	0.20

In the current study, only construction and impoundment load cases are considered, while Ouedraogo et al., [1] include seismic analysis. The load cases considered are adopted from Ouedraogo et al., [1], who assume the construction of the diaphragm wall before the construction of the dam embankment. Displacements, stresses, and strains are calculated by considering the following cases:

- Step 1: “Construction of the diaphragm wall and the plinth”
- The earth pressures and the hydrostatic pressures are balanced on both sides (Upstream-downstream direction) of the diaphragm wall. The diaphragm wall is thus subjected to its own weight, the weight of the plinth, and friction with the alluvium [1].
- Step 2: “Step 1 + completion of the dam and the mask in 10 layers”
- The installation of the embankments for the construction of the dike is done gradually until reaching the crest of the dam. The thrust of the earth due to the weight of the dam downstream of the diaphragm wall induces a movement of the diaphragm wall upstream, in addition to settlement in the alluvial foundation [1].
- Step 3: “Step 2 + Installation of the upstream toe embankment”
- The placement of stringers at the upstream foot of the dam on the head of the diaphragm wall and the plinth constitutes an additional load for the diaphragm wall, causing its settlement and the one of the foundations.
- Step 4: “Step 3 + Impoundment of the dam up to the normal water level”
- To the forces due to load Step 3, are added the hydrostatic weight of the water above the plinth and the hydrostatic thrust resulting from the difference in the hydraulic load between the upstream and downstream of the diaphragm wall [1].

In accordance with the phasing given above, calculations have been made using Plaxis. Ouedraogo et al., [1] reported that has used Plaxis to analyse excavations supported with a diaphragm wall formed with rows of dry deep mixing columns [8]. Plaxis is indeed the model used by Ouedraogo in [1].

3. Results and Discussion

In the following paragraphs, we are going to show in the one hand the results of a similar modeling as studied by [1], to emphasize the accumulation of distortions at the junction points of the diaphragm wall. Then the distribution of displacements will allow us to give an explanation to that phenomenon. Understanding the magnitude and profile of these parameters is crucial for assessing Ouedraogo’s results. Indeed, ground movement potentially affects nearby structures [11]. In the other hand, we will study a geometry-based solution to tackle that issue. Finally, a second external solution will be investigated. This one is based on the planning related to the dike’s construction.

3.1. Structural Behavior of The Diaphragm Wall

The maximum displacements and distortions in the diaphragm wall are summarized in table.2 below. In order to visualize the evolution of the total displacements all along the construction of the dam, we made a plot of each phase. The results are shown on Figure 4. In this figure, Y coordinate are given on the cross section crossing the middle of the diaphragm wall as shown in right side of the figure.

It can be noticed on the figure that the construction of the dike engenders the displacement of the diaphragm wall accordingly. Hence, while the dike is getting higher, the diaphragm wall moves accordingly upstream. This corroborates the results given by Ouedraogo et al., [1]. Two points in the Y coordinate draw our attention: the points around Y=213m and Y=245m.

Although the relatively uniform variation of the displacements, theses to points stand out by the inflexion of all the curses. Indeed, at theses points, it can be noticed a change in the variation rate. Quantitatively, the curves vary smoothly from Y=208m to Y=213m, then the variation rate increases from Y =213m to Y =215m. Then it remains relatively smooth on the body of the diaphragm wall from Y =215m to Y =244m. At this point again, the same phenomenon is noticed: from Y =244m to Y =246m, the variation rate gets higher, and suddenly, decreases from Y =246m to Y =248m. In this last interval, it can be seen that the variation gets even negative, leading to a decrease of the displacement. This is more visible on the impoundment phase (refer to Figure 4). These particular intervals are emphasized on Figure 4 by vertical red barres.

Referring now to the corresponding position of these points on the diaphragm wall, it goes out that they are the anchoring points of the diaphragm wall: the first point is the anchoring with the bedrock (*Y*=213m), and the second is the anchoring with the head block(*Y*=246m). This is a proof

that the accumulation of the distortions at the anchoring points as stated in Ouedraogo et al., [1] is due to the sudden change in the displacement rate. In Figure5, we show the deformed mesh of the diaphragm wall, with emphasis to these two points. Note that the figure shows the true deformation, and an exaggerate one for visualization purposes, to present the deflexion at theses points.

Table 2. Calculation results -maximum deformations-

Load case	Corresponding Phase	U [cm]	Pu [cm]	γ_{xy} [%]	
1	Diaphragm Wall and plinth	1.19	1.19	0.021	-0.018
2	Dike and Mask	47.48	-	0.563	-2.475
3	Foot Embankment	49.09	7.21	0.579	-2.479
4	Impoundment	119.5	125.7	0.585	-2.504

Note: U is the total displacement, Pu is the total phase displacement, and γ_{xy} is the total strain (distortion).

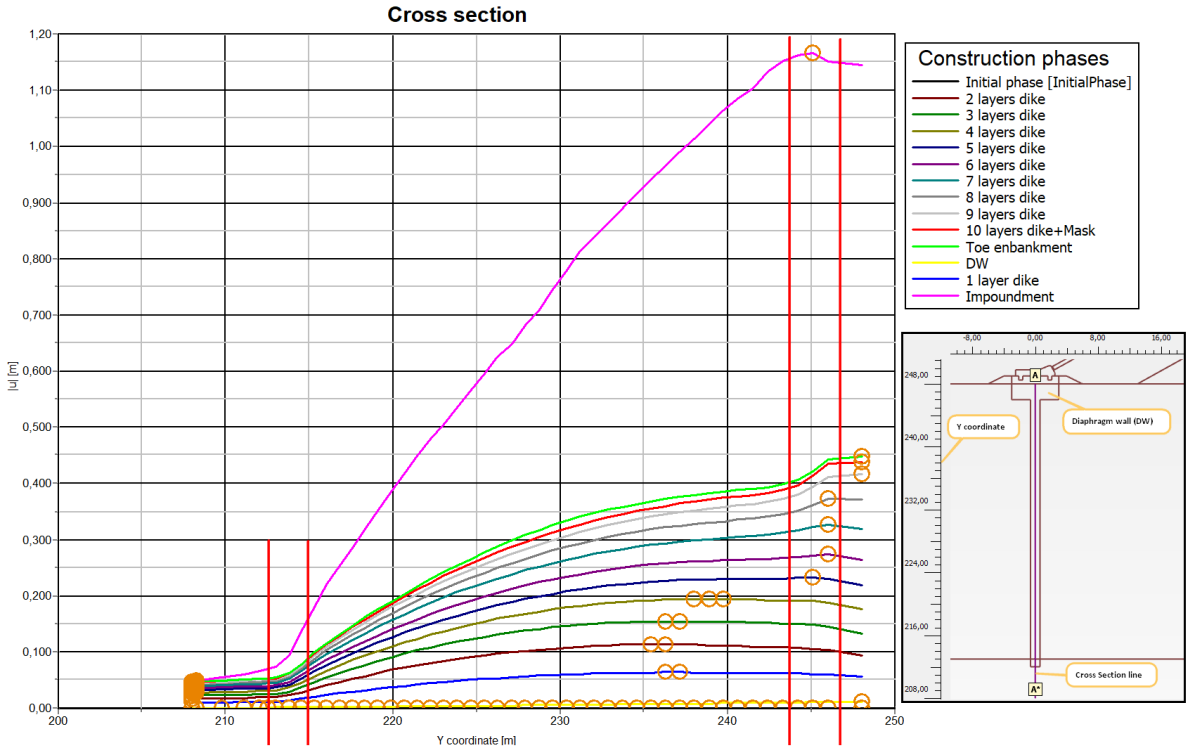

Fig. 4. Cross section of the diaphragm wall showing the evolution of total displacement (U) per phase

To support our point on the relationship between the displacements rate and the distortion accumulating to the junction points of the diaphragm wall, we have plotted the distribution of the distortions along the same cross section as the displacements one. Fig 6 shows that chart.

As it can be easily noticed, the same areas where displacements changed suddenly, the distortions get their maxima. For instance, around the junction points, all the curves get a peak. Although almost the whole curves have the same tendence, the impoundment one (the yellow curve) shows a different behaviour. Indeed, this curve shows, a pic at the middle of the diaphragm wall. Plus, although the pic at the junction points with the bedrock, the sign of the distortions from the bottom of the diaphragm wall (Y=208m) to Y=214,5m is opposite to their sign in the other curves. From Y=214,5m, all the distortions have the same sign.

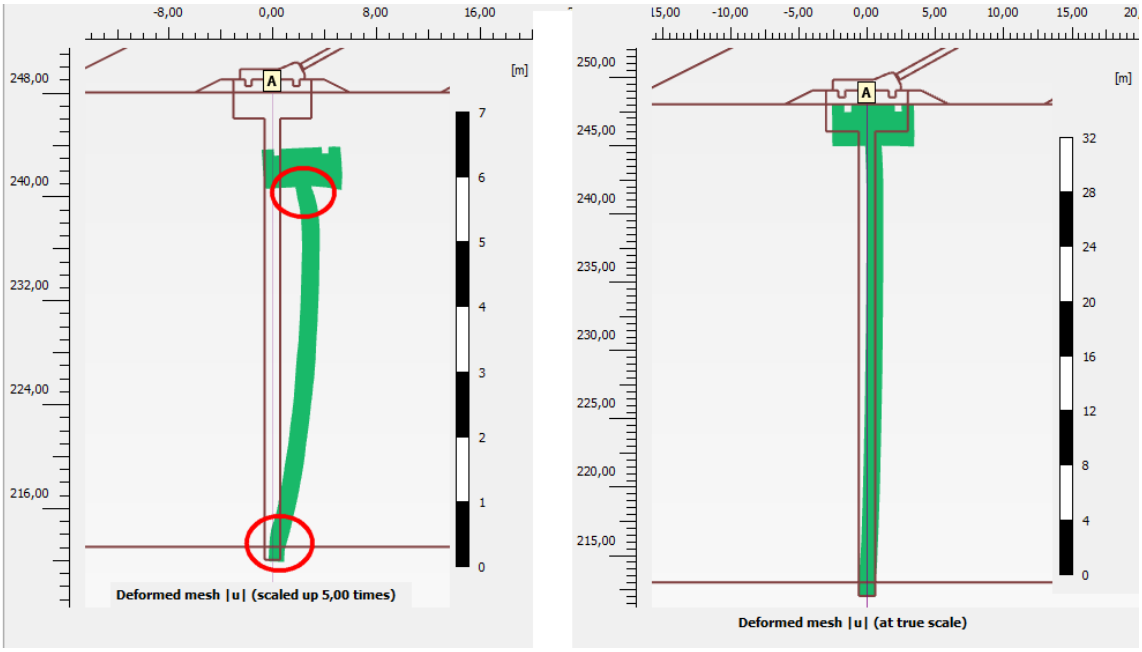

Fig. 5. Deformed mesh of the diaphragm wall at true scale (right) and scaled up 5times(left)

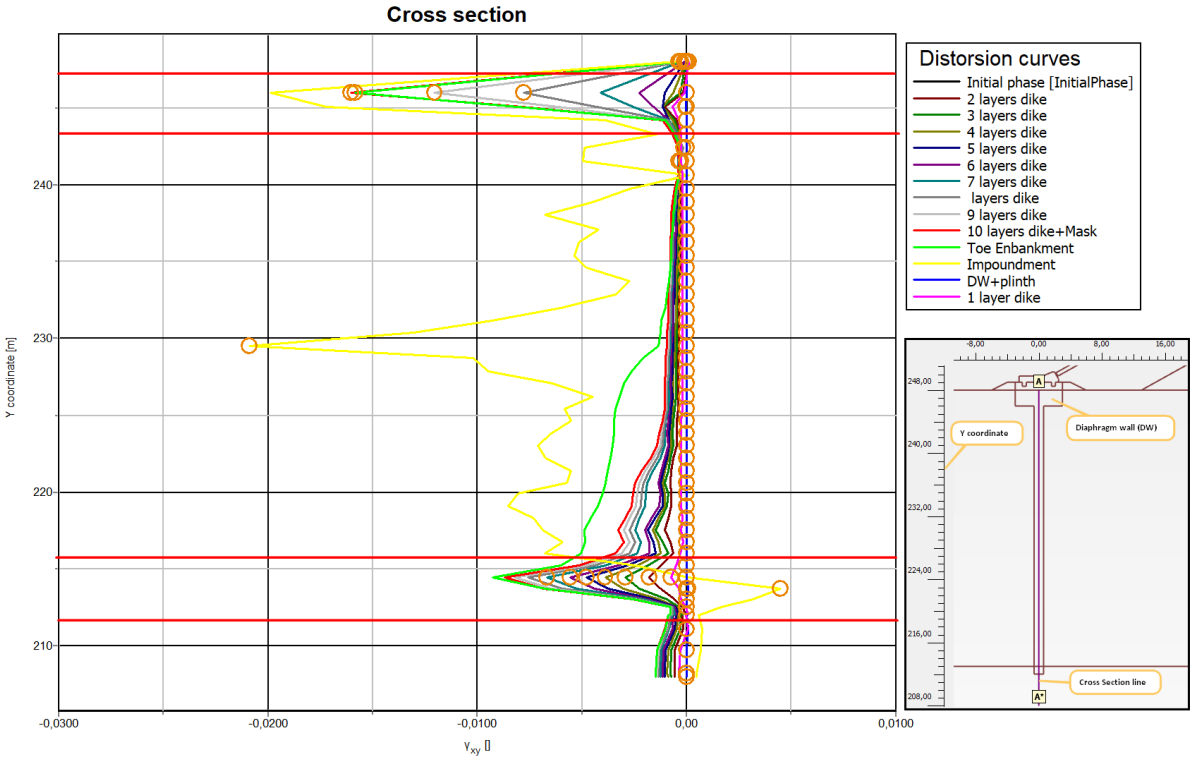

Fig. 6. Distribution of distortions on the body of the diaphragm wall

The change in behaviour of the impoundment curve is not irregular, because the impoundment changes the direction of the displacements in the diaphragm wall: while moving upstream during the dike construction, the diaphragm wall moves downstream during the impoundment. This result is also emphasized in Ouedraogo et al., [1]: "In fact, the hydraulic gradient between the upstream under the load of the reservoir and the almost drained downstream causes the wall to move widely downstream, thus exceeding its original axis". These changes in the displacements' direction explain the changes in the distortions and may be a reason of the impoundment curve's 3rd peak at the middle of the diaphragm wall.

Figures 7 and 8 are plots of the distortions' distribution on the body of the diaphragm wall. Note that only the last two phases are plotted. Figure7 shows the cross sections while Figure 8 shows the distribution on all the diaphragm wall.

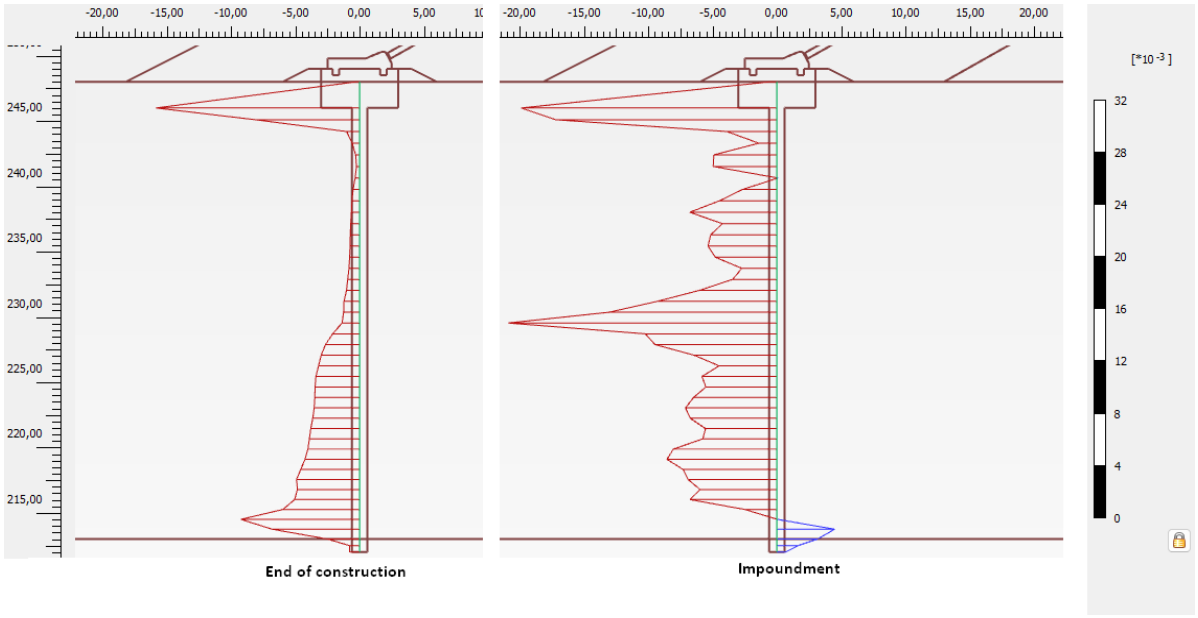

Fig. 7. Distribution of distortions on the body of the diaphragm wall -cross section view-

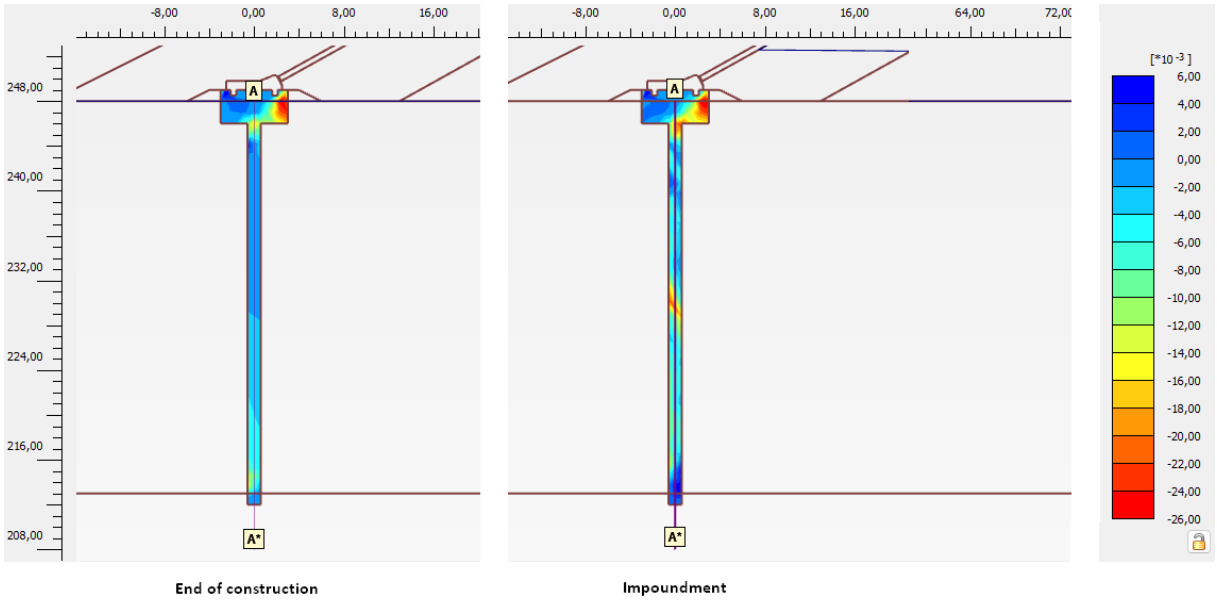

Fig. 8. Distribution of distortions on the body of the diaphragm wall -full chart view-

At this stage of our study, it is assumed that the distribution of displacement causes the diaphragm wall to accumulate strains at its anchoring points. While approaching the bottom point of the diaphragm wall seems difficult at this time of our investigations, here are several effective strategies to tackle the concentration of strains at the junction with the head block and drive meaningful change.

3.2. Effective Approaches to Address the Issue

Two distinct yet complementary approaches to the problem mentioned above are provided in the paragraphs that follow.

3.2.1 Through Geometry Improvement

In this approach, we present a design adjustment to the head block. This new design consists in smoothing the junction, in other to avoid sudden break in the thickness of the diaphragm wall as a whole. Indeed, instead of having 90° joint between the head block and the body of the diaphragm wall, we propose to widen this angle.

3.2.1.1 Definition and Mathematical Concepts of The Approach

Referring to figure 9.a, let θ be the angle $\widehat{BCD}$. We assume to refer to θ as the junction angle. Considering points A and O fixed for design constraints (indeed, the area above O is supposed to be the anchor of the plinth), and 90° as the minimum value of θ, the angle θ can be widened by moving point B upward and/or moving C downward. In order to maintain an equal surface of the diaphragm wall, our approach consists in movement B at point B'=O and bringing down point C at C' as indicated on Fig 9. (b)

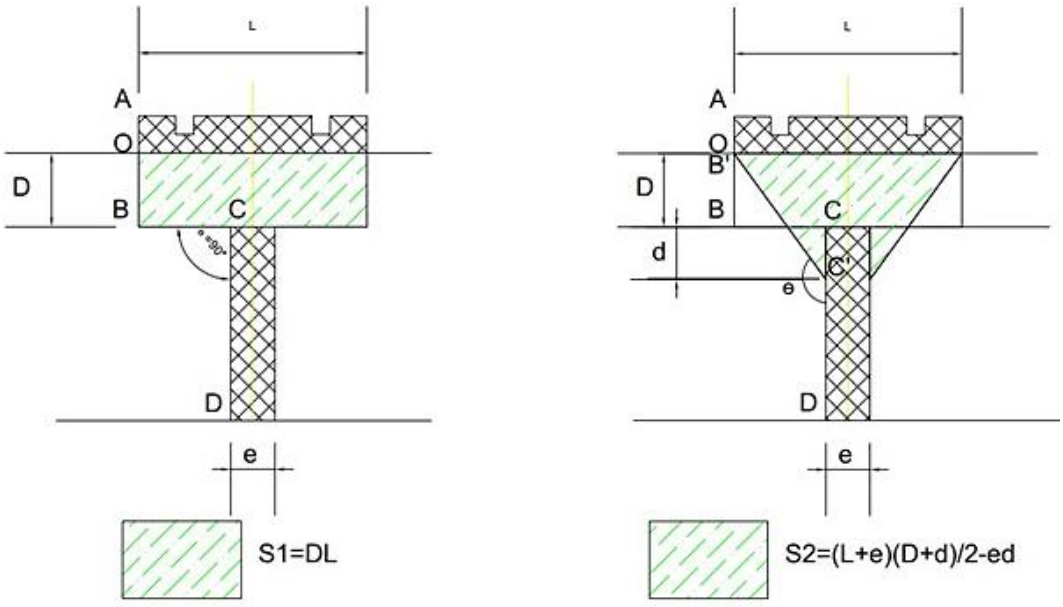

(a) (b)

Fig. 9. Definition of the junction angle ɵ : (a) ɵ=90°, (b) for any value of ɵ

The surface modification induced by the change in geometry concerns exclusively the surfaces *S1* and *S2*, as illustrated in Figure 9 a and b. Assuming parameters *L, D* and *e* fixed, to have the same surface from fig 9.a to fig 9.b ($S1 = S2$), we have to solve equation (2) for *d* (Note that the reason of the assumption "$S1 = S2$" is given at the end of paragraph 0).

$$D.L = \frac{(L+e).(D+d)}{2} - e.d \tag{2}$$

Where *L, D, e* and *d* are as defined on figure 9. Equation (2) can be simplified by solving for d, resulting in:

$$d(L-e) = D(L-e) \tag{3}$$

In practical applications, the value of $\boldsymbol{L}$ is greater than $\boldsymbol{e}$. Indeed, for CFRD dams' application, $\boldsymbol{e}$ varies from 1 to 2m while $\boldsymbol{L}$ is greater than 5m. Then, equation **(3)** can be divided by $(\boldsymbol{L}-\boldsymbol{e})$ leading to the result bellow:

$$L \gg e \Rightarrow (L-e) > 0 \tag{4}$$

$$(3)\ \&\ (4) \Longrightarrow d = D \tag{5}$$

So, having the same surface requires distance BB' equal to distance CC'. This can be geometrically interpreted as a 180° rotation of triangle OBO' around point O' both sides of the diaphragm wall as shown on Figure 10.

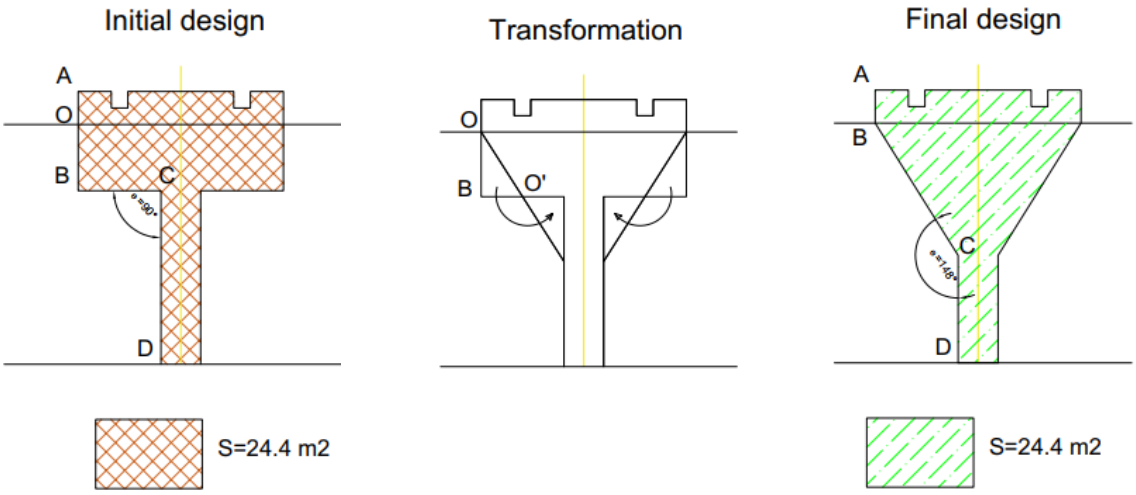

Fig. 10. Geometrical interpretation of the approach

From the results and figures above, a general expression of the junction angle $\boldsymbol{\theta}$ can be established as follows:

$$tan(\pi-\theta)=\frac{\frac{L-e}{2}}{D+d}=\frac{L-e}{2(D+d)} \Leftrightarrow \pi-\theta=atan\left(\frac{L-e}{2(D+d)}\right) \Leftrightarrow \theta=\pi-atan\left(\frac{L-e}{2(D+d)}\right) \quad (6)$$

$$\theta=\pi-atan\left(\frac{L-e}{2(D+d)}\right)$$

In the current study, the numerical values avec the parameters are as follow: $L=6.2m\,;e=1.2\text{m}\,;D=d=2.0\text{m}$. This leads to: $\theta=\pi-\text{atan}\left(\frac{6,2-1,2}{2*4}\right)=\pi-atan(0,625)\simeq 2.58299rad\asymp 148°$

3.2.1.2 Numerical Modelling and Analysis of The Solution

In this section, we are going to show the results of the numerical analysis of the solution described above. For practical raisons, we will focus on the two first and two last phases, meanwhile the diaphragm wall 's construction (Phase_1), the first 8.5m layer of the dike (Phase_2), the last construction phase (end of construction) and the impoundment phase. The analysis will consist in comparing the results of the new geometry (Solution 1) to the initial one studied by OUEDRAOGO et al., [1]. Due to Plaxis software restrictions, the curves have been plotted with excel software. Indeed, Plaxis doesn't allow plotting data from different projects files. So, the results have been copied from Plaxis to excel. Fig. 11 shows the displacements' curves of the initial geometry (Initial) and the solution described above (Solution 1).

Note that the curves with a square point type refer to the solution described above while the ones with cross type refer to the initial design. In a general view, the curves of the two designs have the same behavior. Still, some differences hide behind the details. Indeed, when we take a close look at the curves, some changes appear around the junction between the head block and the body of the diaphragm wall. For visual reasons, we have plotted only the two last phases around the junction on Figure 12.

As it can be seen on Figure 12, the curves' variation rate changes differently around the junction:

- End of construction phase: as for this phase, we note that the initial design's curve presents a sudden increase around Y=245m (remember that the junction is at Y=246m), while the Solution 1 design barely changes its behavior.
- Impoundment phase: although the two curves start decreasing the junction, each curve does it in a different way. Indeed, as shown on Figure12 ant Table 3, Solution 1 curve decreases

0,71% while Initial curve decrease 2,22%. The decrease of the two curves may seem tiny in terms of length, but seen from the rate perspective, Initial curve decreases 3 time faster than Solution 1 one. This result is particularly interesting given that these changes happen around the junction point.

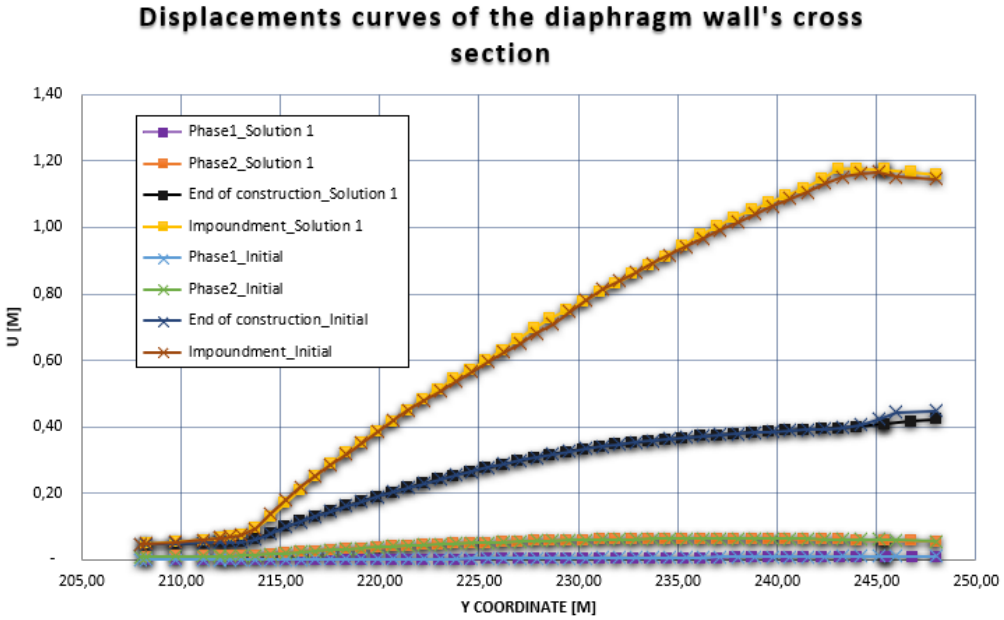

Fig. 11. Comparative curves of the displacements at the cross section of the diaphragm wall

Table 3. Variation rate of Initial and Solution 1 curves around the junction.

	$Y1$ (m)	$Y2$ (m)	ΔY (m)	$U1$ (m)	$U2$ (m)	ΔU (m)	$\frac{\Delta U}{\Delta Y}$ (%)
Initial	245.1	246.0	0.90	1.17	1.15	0.02	2.22
Solution 1	244.0	245.4	1.40	1,18	1,17	0.01	0.71

Note: $\Delta Y = Y2 - Y1$ and $\Delta U = U2 - U1$

These observations will help us to explain what happens in terms of distortion. Indeed, as we did with the displacements, we have plotted bellow the distortions' curves of the two designs (Initial and Solution 1) from the two last phases. Fig 13 shows the strains' (distortions') curves of the initial geometry (Initial) and the solution described above (Solution 1). The red circles and lines on the graph of Figure 13 emphasizes the distortions' peak areas on the diaphragm wall.

This graph shows that the peak at the junction point with the head block has been cleared in the Solution 1 design. Indeed, while the initial geometry's curves show a peak around Y=244m and Y=247m, the curves of Solution 1 show almost no change between the body of the diaphragm wall and the head block. Thus, smoothing the junction angle is an effective strategy to prevent distortion at the connection between the head block and the diaphragm wall's body. This proactive approach safeguards structural integrity for long-lasting performance.

By the way, this solution miraculously eliminates the peak at the middle of the diaphragm wall. Indeed, as we can see on Figure 13, the peak at the middle of the diaphragm wall is mitigated (from 2.1% to only 0.45%). However, it is essential to highlight that the impoundment curve's first peak at the junction with the bedrock has slightly increased (from 0,45% to 0,85%). Anyway, the new design's distortions never reach 1.0% (they vary from -0,95% to 0,85%) while the initial ones reach -2.1%.

- Figures 14 and 15 are plots of the distortions' distribution on the body of the diaphragm wall modeled with the smoothed junction angle's geometry for the last two phases. Figure14 shows the cross sections while Figure 15 shows the distribution on all the

diaphragm wall. Fig 15 shows a grouped view of the two geometries results. If $\theta < 148°$ then $S1 > S2$: this is a cheaper variant of our design (Solution 1), but is also less efficient,

- If $\theta = 148°$ then $S1 = S2$, corresponding to our design (Solution 1), described and analysed above,
- If $\theta > 148°$ then $S1 < S2$: in this case, the solution is more efficient but also more expensive.

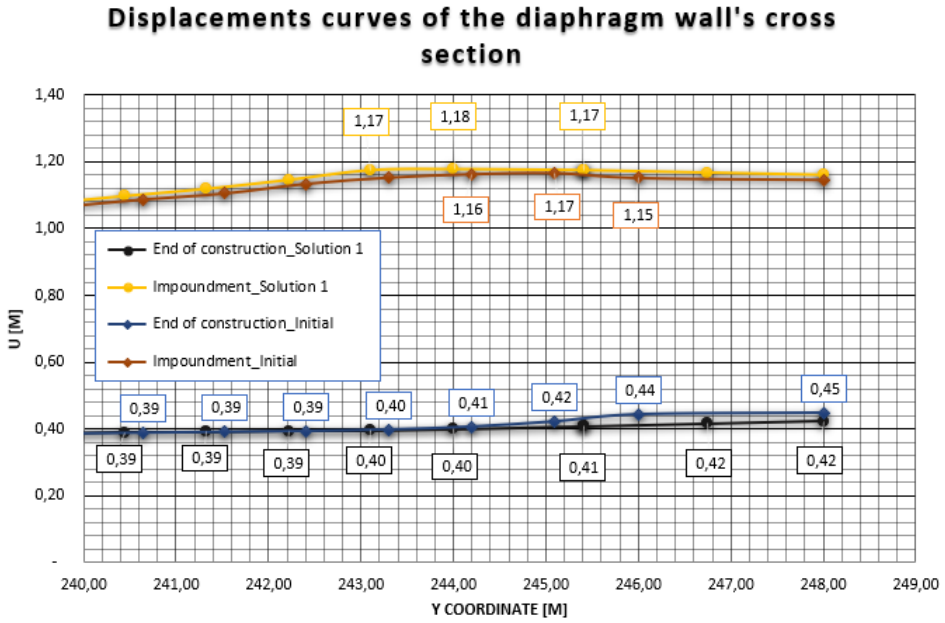

Fig. 12. Focus on last phases curves of the displacements

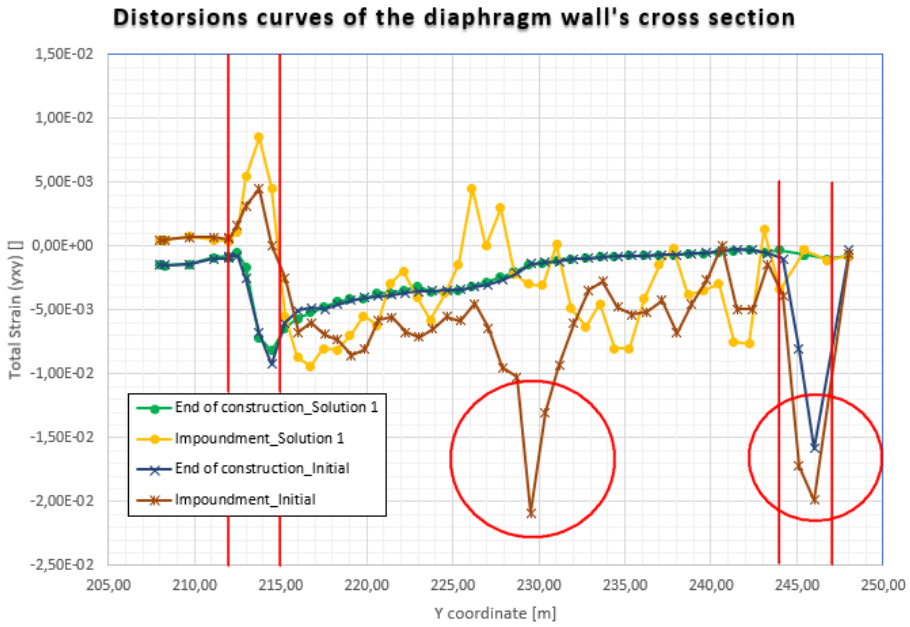

Fig. 13. Focus on last phases curves of the displacements

Now that our solution has proven itself, it is appropriate to clarify some assumptions that guided our approach. Specifically, when defining the junction angle, we assumed that surfaces S1 and S2, as depicted in Figure 9 a and b, should be equal. This assumption was not made randomly. Indeed, the amount of concrete required for this section of the plinth is determined by multiplying this surface area by the length of the plinth in the bank-to-bank direction. So, having these surfaces equal therefore ensures equality of cost between the two designs.

Furthermore, it is possible to evaluate the junction angle in terms of both cost-effectiveness and overall performance:

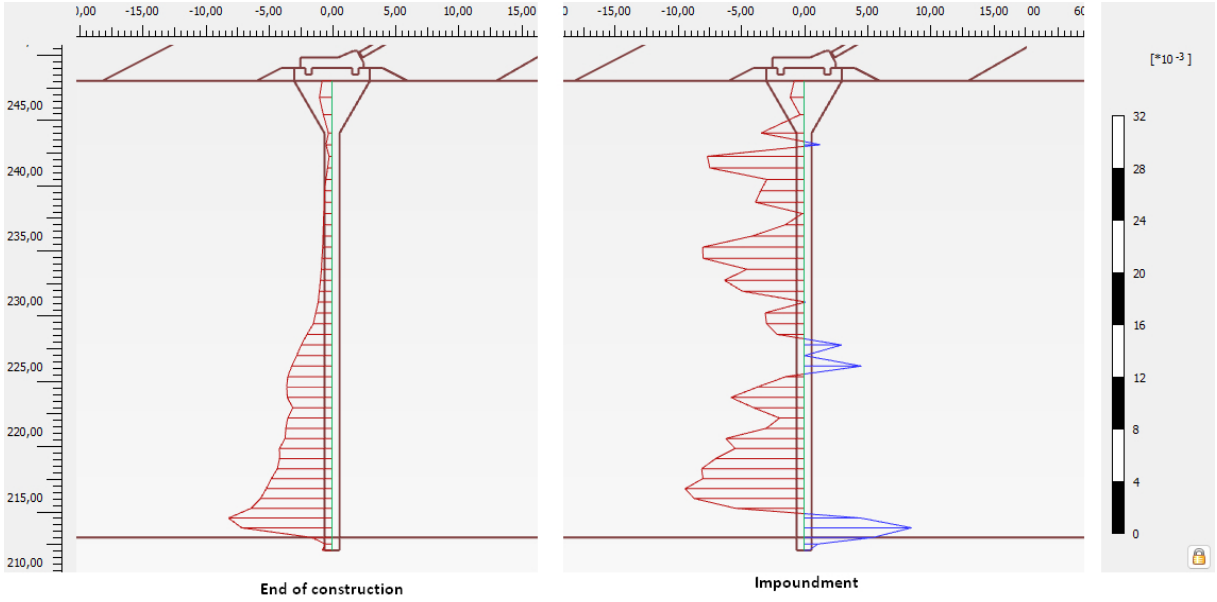

Fig. 14. Cross section view of the distortions' distribution on the body of the diaphragm wall - improved geometry-

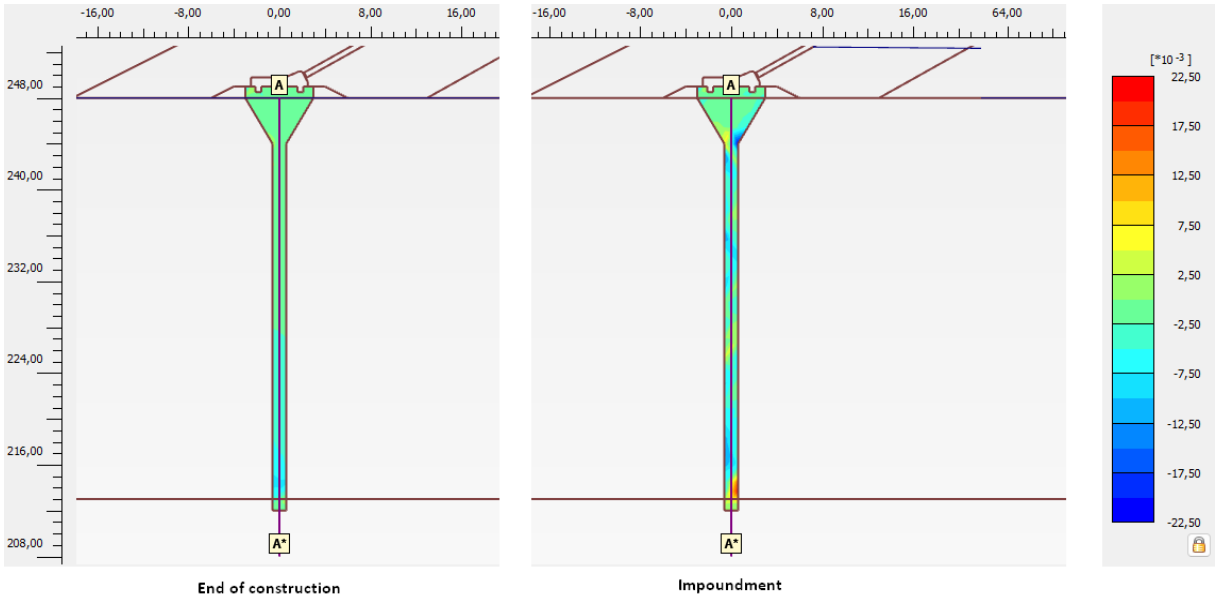

Fig. 15. Distribution of distortions on the body of the diaphragm wall -full chart view-

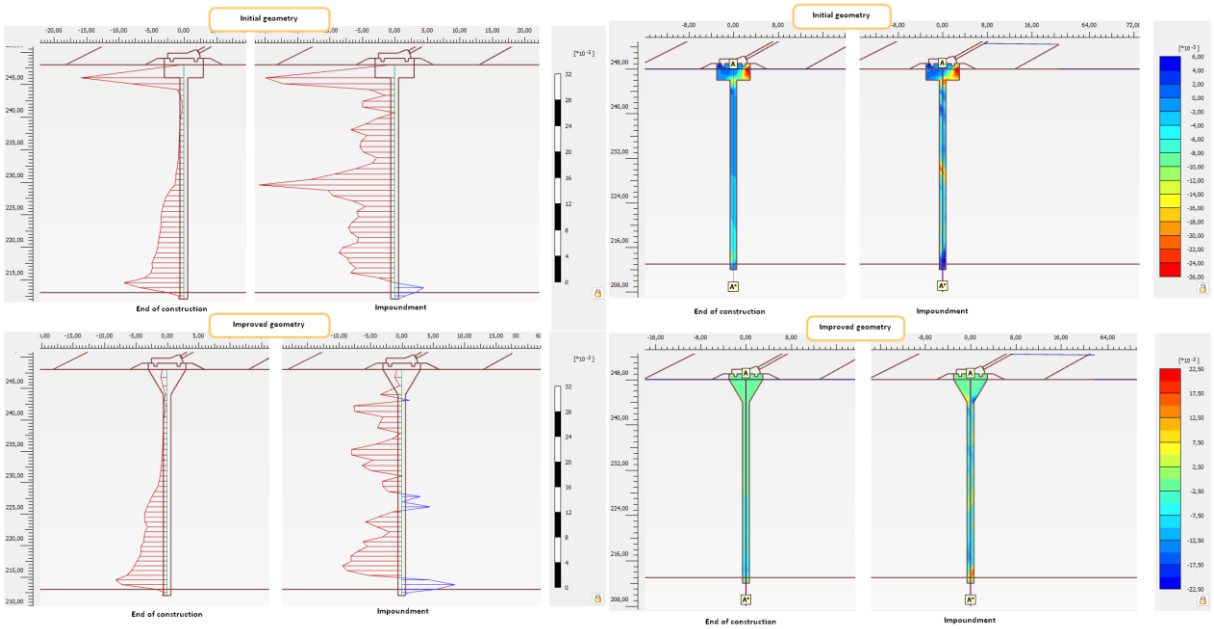

Fig. 16. Comparative views of initial and solution 1 ‘s distortions’ cross sections and cart

3.2.2 Through Planning the Dike Construction

This paragraph analyses a simple attempt to reduce the accumulation of deformations at the junction point by gradually charging the diaphragm wall. Indeed, as we are going the show, the peaks of distortions can be mitigated by planning strategically the dike’s construction.

To demonstrate that, we will compare the distortions field of two different ways of constructing the dike. For instance, it is necessary to present these ways of construction.

3.2.2.1 Geometrical Concept

The classic way consists in constructing the dike by full horizontal layers form upstream to downstream. Our approach consists in starting the dike’s construction at a certain distance from the diaphragm wall. This, to let the soil layer reorganize at a sufficient distance from the diaphragm wall in order to affect its body smoothly from the bottom to the head. For this application, we have chosen to begin the dike 10m far from the diaphragm wall for the first 4 layers of the dike.

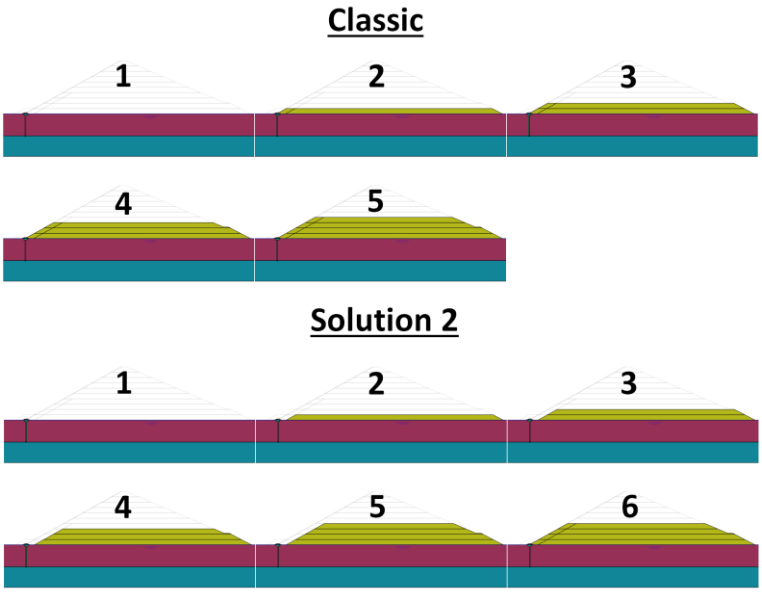

Fig. 17. Presentation of the two ways of the dike’s construction

Figure 17 shows the process of the dike's construction in the two ways. "Classic" is the way usually applied to construct dikes while "Solution 2" refers to our approach. Note that the figure only shows the first 4 layers of the dike. The next steps of the construction are the same, with each layer constructed as a whole. In the following, these two solutions are numerically simulated, and their results compared.

3.2.2.2 Analysis, Results, And Discussion Around the Two Planning's

This section focuses on the comparison of the distortions field of the two solutions. This comparison makes it possible to observe the reduction of distortions at the diaphragm wall's critical points. To focus on the principal results, we are going to show in the one hand the maximum displacements of the diaphragm wall in the two cases, and in the other hand, their distortions.

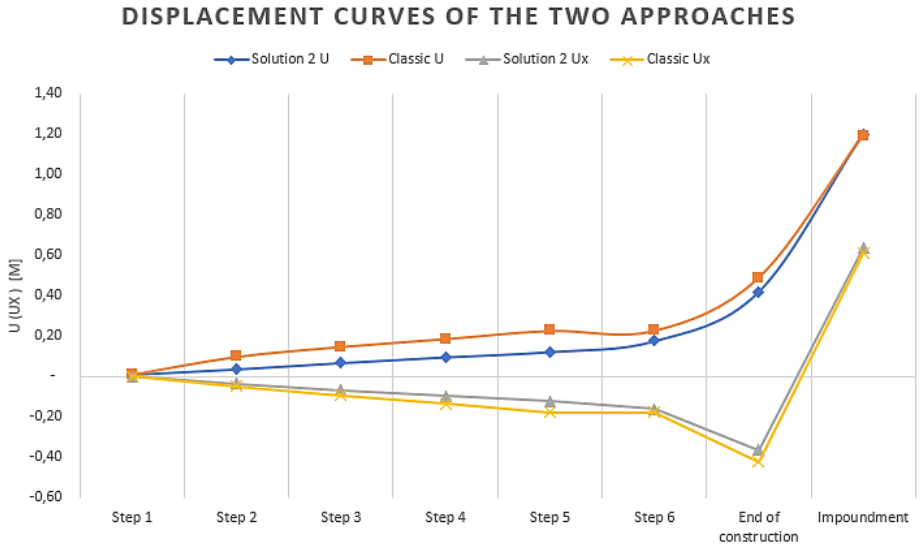

Fig. 18. Maximum displacements in the diaphragm wall U is the total displacement while Ux is the horizontal displacement

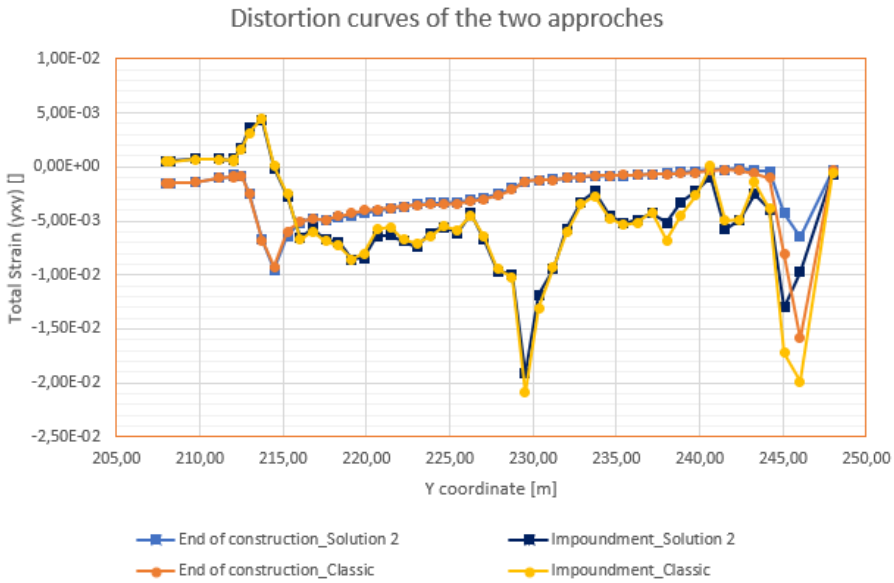

Fig. 19. Cross section of the diaphragm wall showing the distortions curves of the approaches

Figure 18 shows the maximum displacement curves of each approach. Note that Step 1 to 6 are as depicted on Figure 17. As it is easy to notice, the displacements curves of the Solution 2 approach are under the one of the Classic approaches for all the steps instead of impoundment. Meanwhile, during the dike's construction, the diaphragm wall is more deformed in the Classic process than in

The Solution 2 process. Note that this result is true for maximum displacement (U) and horizontal maximum displacement (Ux). Ux is negative because the diaphragm wall displaces upstream [1]. Nevertheless, the displacements are the same in the two approaches for the impoundment step. This is not a random outcome: in fact, it is the same state of constraints in the dam just before impoundment for the two cases. Coming now to the distortions, the results show that proceeding by Solution 2 process can help reduce the amount of the strains at the peaks. Fig 19 shows a comparative view of distortion curves of the two approaches. As we did in previous analysis, focus is made on the last phases: end of construction and impoundment.

According to the results shown on Figure 19, the distortions along the body of the diaphragm wall are almost the same for the two approaches, except some rare differences. Indeed, the curves related to the end of construction stage are nearly identical for the two approaches: the peaks happen at the same points and the values otherwhere are practically the same.

However, the values at the peaks make the difference. Solution 2 curves' peaks' values are less high than Classic ones. Indeed, when having a close glance to the peaks of the curves, we come to see that they (the peaks) are reduced from the top to the bottom of the diaphragm wall:

- Top peak : the peak at the head block junction is reduced more than a half at the end of construction in Solution 2 approach compared to it's value in Classic approch. Impoundment curves show a similar result, with the value reduced from a third;
- Middle peak : the peak occuring after the dam impoundment at the middle of the diaphragm wall remain on the two approaches. Anyway, we note a slight decrease from classic to solution 2 curves. No peak happens during the construction phase at the middle of the diapgragm wall;
- Bottom peak : finally, the peak at the bedrock junction of the diaphragm wall remain unchanged in the two approches, with nealy no anhancement.

These results show that starting the dam embankment at a certain distance from the diaphragm wall is a simple way to enhance its integrity by reducing both displacements and distortions. The results also show that the reduction of distortions is more pronounced at the top of the diaphragm wall and decreases from top to bottom. This effect may be due to the distance from which de embankment is started. While the current study shows the effect for 10m far from the diaphragm wall, starting at a longer distance may lead to more interesting results.

4. Conclusion

Based on numerical simulation, a diaphragm wall set upstream a high dam has been studied in this paper. The paper tackles a structural integrity issue highlighted by a recent similar study result. Indeed, in his 2025 study, OUEDRAOGO has raised the problem of concentrating distortions at critical points of soft diaphragm walls set on thick alluvium layers. The study consisted of investigating about that issue.

It comes out from the study that the concentration of distortions at the junction points (reaching 2%) is real and harmful to the diaphragm wall's long-lasting performances. Then, this paper proposed two effective ways to deal with the issue. Indeed, in the one hand, the paper proposes to smooth the junction angle between the head block and the body of the diaphragm wall. This simple and costless measure has proven significant results, helping to eliminate the distortions' concentrations at the upper junction point. The final distortion at the junction is only 0,1%. Plus, it helps in reducing another distortion peak that happens at the middle of the diaphragm wall, from 2,1% to 0,45%.

In the other hand, the paper demonstrates that strategically planning the dike construction is an effective way to deal with the same issue. Indeed, by starting the dike's construction far from the diaphragm wall, it is proved that the concentration of distortions around the junction point is mitigated. Although this trick helps to mitigate the concentration of strains during the construction stage, the impoundment phase requires a smooth junction point to avoid peaks on that junction and elsewhere on the diaphragm wall.

In sum, combining both solutions are highly recommended to effectively enhance the structural integrity of the diaphragm wall and ensure its durability for the long term. This integrated approach not only strengthens performance but also instills confidence in the diaphragm wall's longevity. Still, the anchoring point with the bedrock deserves to be investigated. The two solutions investigated above are yet incapable of reducing the concentration of distortions at this lower junction point.

Acknowledgement

I would like to thank Pr Latifa Ouadif for her indefectible help and comprehensiveness which lead to the realization of this work. I also thank Pr Anas Bahi for all the support he provides to me for my work. Finally, many thanks to everyone who helped me achieve this paper. A special thought to my wife and Dr Eddie Nébié.

References

[1] Oudraogo I, Ouadif L, Bahi A. Diaphragm wall behaviour under thick alluvium layer conditions. Civil Environ Eng. 2025;21(1):CEE_072524. https://doi.org/10.2478/cee-2025-0005
[2] Zhang J, Li M, Ke L, Yi J. Distributions of lateral earth pressure behind rock-socketed circular diaphragm walls considering radial deflection. 2022; 104604. https://doi.org/10.1016/j.compgeo.2021.104604
[3] He W, Luo C, Cui J, Zhang J. An axisymmetric BNEF method of circular excavations taking into account soil-structure interactions. 2017; 90:155-163 https://doi.org/10.1016/j.compgeo.2017.06.001
[4] Shao Y, Chen C, Lu Z, Zheng Y, Zhang Y. An intelligent leakage detection method for diaphragm wall joints based on fiber Bragg grating sensors and intelligent algorithms. 2022; 197; 111339. https://doi.org/10.1016/j.measurement.2022.111339
[5] Sari M, Seren A, Alemdag S. Determination of geological structures by geophysical and geotechnical techniques in Kirklartepe dam site (Turkey). 2020. https://doi.org/10.1016/j.jappgeo.2020.104174
[6] Boettinger JL. Alluvium and alluvial soils.Encyclopedia of Soils in the Environment. 2005; 45-49. https://doi.org/10.1016/B0-12-348530-4/00008-4
[7] DeJong JT, Sturm AP, Ghafghazi M. Characterization of gravelly alluvium.Soil Dynamics and Earthquake Engineering. 2016; 91:104-115. https://doi.org/10.1016/j.soildyn.2016.09.032
[8] Ignat R, Baker S, Larsson S, Liedberg S. Two and three-dimensional analyses of excavation support with rows of dry deep mixing columns. Computers and Geotechnics. 2015; 66: 16-302015. https://doi.org/10.1016/j.compgeo.2015.01.011
[9] CIGB-ICOLD. Bulletin 141: Concrete face rockfill dam: concepts for design and construction. 2010.
[10] CIGB-ICOLD. Bulletin 51: Matériaux de remplissage pour coupures étanches = Filling materials for watertight cut off walls. 1985.
[11] Aung AY, Kamchoom V, Aye ZZ. Diaphragm wall lateral movement in deep excavations in Bangkok clays: impacts and influencing factors. Can Geotech J. 2024.
[12] CIGB-ICOLD. Bulletin 150: Cutoffs for dams. CRC Press 2018. https://doi.org/10.1201/9781351035989
[13] CFBR. Recommandations pour la justification des barrages et des digues en remblai = Guidelines for the justification of embankment dams and levees. 2015.
[14] Mohamed B, Bahi L, Ouadif L, Bahi A, Sabihi A. Determination of vibro-compaction parameters by making a test board in a port site in Morocco. Civil Environ Eng. 2023;19(1):328-38. doi:10.2478/cee-2023-0029. https://doi.org/10.2478/cee-2023-0029
[15] Hanh DK, Truong DD, Bui KT. Application of numerical modeling and GIS for simulating inundation under dam failure scenarios. Civil Environ Eng. 2024;20(1):233-54. https://doi.org/10.2478/cee-2024-0019
[16] Berkat B, Akhssas A, Ouadif L, Bahi A. Assessment of liquefaction potential by comparing semi-empirical methods based on the CPT test. Civil Environ Eng. 2024;20(1):164-79. https://doi.org/10.2478/cee-2024-0014
[17] Hruban K. Methods of foundation engineering. Chapter 10. 1979.
[18] Souileh A, Mabrouk A, Ouadif L, El Hachmi D. Analysis of the geotechnical and mineralogical characteristics of the Settat-Khouribga shale clay for potential civil engineering applications. Res Eng Struct Mater. 2024;10(4):1699-716. https://doi.org/10.17515/resm2024.408ma0824rs
[19] Souileh A, Mabrouk A, Ouadif L, El Hachmi D, Chrachmy M, Benhaddou K. Building earthquake resilience with clay shale: pioneering sustainable concrete solutions with ecofriendly materials. Res Eng Struct Mater. 2024;10(4):1717-31. https://doi.org/10.17515/resm2024.479ea1007rs